

2020-11-15

# Reduced Arctic sea ice extent during the mid-Pliocene Warm Period concurrent with increased Atlantic-climate regime

Rahaman, W

<http://hdl.handle.net/10026.1/16216>

---

10.1016/j.epsl.2020.116535

Earth and Planetary Science Letters

Elsevier BV

---

*All content in PEARL is protected by copyright law. Author manuscripts are made available in accordance with publisher policies. Please cite only the published version using the details provided on the item record or document. In the absence of an open licence (e.g. Creative Commons), permissions for further reuse of content should be sought from the publisher or author.*

# **Reduced Arctic sea ice extent during the mid-Pliocene Warm Period concurrent with increased Atlantic-climate regime**

\*Waliur Rahaman<sup>1</sup>, Lukas Smik<sup>2</sup>, Deniz Köseoğlu<sup>5</sup>, Lathika N<sup>1</sup>, Mohd  
Tarique<sup>1</sup>, Meloth Thamban<sup>1</sup>, Alan Haywood<sup>3</sup>, Simon T. Belt<sup>2</sup>, J. Knies<sup>4,5</sup>

<sup>1</sup>National Centre for Polar and Ocean Research (NCPOR), Ministry of Earth  
Sciences, Vasco-da-Gama, Goa 403804, India

<sup>2</sup>School of Geography, Earth and Environmental Sciences, University of  
Plymouth, PL4 8AA, UK

<sup>3</sup>School of Earth and Environment, University of Leeds, Woodhouse Lane,  
Leeds, LS2 9JT, UK

<sup>4</sup>Geological Survey of Norway, N-7491 Trondheim, Norway

<sup>5</sup> CAGE – Centre for Arctic Gas Hydrate, Environment and Climate,  
Department of Geosciences, UiT The Arctic University of Norway, 9037  
Tromsø, Norway

**Revised submission to Earth and Planetary Science Letter (EPSL)**

\*Corresponding author ([waliur@ncpor.res.in](mailto:waliur@ncpor.res.in))

Orchid ID: <https://orcid.org/0000-0001-6439-4529>

## Abstract

Quantifying the contribution of poleward oceanic heat transport to the Arctic Ocean is important for making future sea ice and climate predictions. To highlight its potential importance in a warmer world, we present a new record of water-mass exchange between the Atlantic and the Arctic Oceans using the authigenic neodymium isotopic composition of marine sediments from the Fram Strait during the past ~3.4 to 2.6 Ma. In this study, we target the mid-Pliocene Warm Period (mPWP: 3.264–3.025 Ma) of the Pliocene epoch, the most recent geological analogue for future climate change. We complement our semi-quantitative water mass exchange reconstruction with estimates of spring sea ice concentration based on source-specific biomarkers. Our estimates of volume transport of warm waters into the Arctic Ocean suggest long-term secular changes from the lowest during the Marine Isotope Stage M2 “glacial” (3.312–3.264 Ma), to near complete “Atlantification” of the Eurasian sector of the Arctic Ocean during the mPWP. Orbital forcing is found to be the dominant controlling factor for modulating northward volume transport of Atlantic-derived water masses, with an associated reduction in Arctic spring sea ice concentration of ~30-35%. Current generation models often produce diverging results, however, and have not yet been validated against proxy data in northern high latitude settings during the mPWP. Our new results of northward volume transport and sea ice extent therefore provide much needed input for validation of current generation models aimed at improving the robustness of future climate modelling in the Arctic.

**Keywords:** mid-Pliocene, North Atlantic Current, Arctic, Sea ice, Atlantification

## 1. Introduction

The most dramatic changes observed in the Arctic Ocean during the recent past are the unprecedented reductions in sea ice extent and thickness (Kinnard et al., 2011). Although coupled ice-ocean model simulations suggest that the recent warming in the Northern Hemisphere is responsible for this decline (Petrie et al., 2015), there is disagreement between data and models over the impact of atmospheric warming versus oceanic heat transport on sea ice decline (Ding et al., 2018; Dowsett et al., 2012; Haywood et al., 2013). Studies based on proxy reconstructions of heat and volume transport through the Fram Strait (Spielhagen et al., 2011), and in-situ observations in the eastern Arctic Ocean (Polyakov et al., 2017), suggest that enhanced oceanic heat transport by the North Atlantic Current (NAC) over the past few decades likely explains the weakened stratification, increased vertical mixing and reduced sea ice in the Atlantic sector of the Arctic, collectively termed “Atlantification” (Polyakov et al., 2017; Spielhagen et al., 2011). In order to improve our understanding about Arctic sea ice variability, particularly within the current context of rapid global warming, it is imperative to reconstruct sea ice conditions during previous warm climate states, and decipher the underlying mechanisms that control its distribution. One such period in Earth’s history is the Pliocene (5.33–2.58 Ma), which experienced higher global temperatures than pre-industrial (Dowsett et al., 2009), and was characterized by a gradual transition from relatively warm climates during the Early Pliocene towards cooler conditions in the Late Pliocene. Some previous organic geochemical-based proxy climate reconstructions for the Pliocene have been conducted for the North Atlantic and Fram Strait (Clotten et al., 2018; Knies et al., 2002), and similar studies have been carried out for other warm

interglacials such as the Eemian (Marine Isotope Stage (MIS) 5e) and the early Holocene (Belt et al., 2015; Müller et al., 2012; Stein et al., 2017). However, the roles of atmospheric warming versus northward heat transport in controlling sea ice conditions were not assessed as part of these studies.

Here we aimed to identify the potential impact of future changes in oceanic heat transport into the Arctic Ocean and the effects of “Atlantification” in a warmer than modern climate. To achieve this, we conducted a semi-quantitative assessment of northward volume transport of Atlantic water through the Fram Strait during a geological period when (1) climatic conditions in terms of temperature and atmospheric CO<sub>2</sub> level were analogous to modern/or future projected scenarios and (2) global oceanographic and tectonic settings were nearly identical to today. The mid-Pliocene Warm Period (mPWP: 3.264–3.025 Ma) is known to be warmer (globally) than today (Dowsett et al., 1992; Haywood et al., 2016), with atmospheric CO<sub>2</sub> concentrations estimated to be in the range 350–450 ppmv (Berends et al., 2019; Foster et al., 2017). Hence, the mPWP has been proposed as a possible reference for future warm climate states (IPCC, 2013). Confirmation of increased polar ocean heat transport and reduced sea ice in the Arctic Ocean during the mPWP (Raymo et al., 1996) would therefore be of clear benefit for the assessment of coupled ocean-ice-atmosphere model simulations of the mPWP (Haywood et al., 2016).

To achieve this objective, we first reconstructed an orbital-resolution record of watermass mixing between the NAC and Arctic-derived polar waters (PW) in the Fram Strait (Fig. 1), based on authigenic neodymium (Nd) isotopes ( $\epsilon_{\text{Nd}}$ ). The radiogenic isotope composition of Nd in seawater reveals changes in watermass mixing and

circulation patterns due to its quasi-conservative behavior (Martin, 2002) and lower average oceanic residence time (360–2000 years) compared to the global ocean mixing time ~1500 years (Tachikawa et al., 1999) . Critically, in contrast to stable oxygen ( $\delta^{18}\text{O}$ ) or carbon isotope ( $\delta^{13}\text{C}$ ) measurements, the Nd isotope ratios are not affected by isotopic fractionation resulting from any biological or other low-temperature processes, so represent a robust proxy for paleo-water mass circulation (Martin, 2002). In a modern context, the majority of Atlantic-derived water masses are transported northward into the Arctic Ocean along the Svalbard continental margin, which is the northernmost extension of the NAC (Fig. 1). This warm water submerges into the Arctic Ocean or is deflected westward and submerged southward below cold and less saline waters of the East Greenland Current (EGC). All of these modern water masses possess characteristic Nd isotope signatures (Fig. 1) (Laukert et al., 2017; Werner et al., 2014). Less radiogenic values are indicative of a stronger influence of NAC flowing into the Nordic Seas (present-day  $\epsilon_{\text{Nd}} = -13.2$  to  $-13.0$ ) (Teschner et al., 2016) while more radiogenic Nd isotope signatures reflect enhanced contribution from Arctic-derived polar waters (PW) (Laukert et al., 2017) (e.g.  $\epsilon_{\text{Nd}} = -9.9$ ). For this study, an orbital-resolution (~5 ka) authigenic  $\epsilon_{\text{Nd}}$  record was obtained through analysis of bulk sediments from Ocean Drilling Program (ODP) Hole 910C (hereafter referred to 910C) on the Yermak Plateau, eastern Fram Strait, (80°15.894'N, 6°35.430'E, water depth: 556.4 m) covering the interval between 3.4 Ma and 2.6 Ma. This new record is supplemented by a previously published low-resolution (60-70 ka) record of authigenic  $\epsilon_{\text{Nd}}$  from ODP Hole 911A (80° 28.466' N, 8° 13.640' E, water depth: 902 m) (hereafter referred to 911A) at the eastern flank of the Yermak Plateau (Teschner et al., 2016).

To identify the corresponding changes in sea ice coverage and carbonate chemistry, the sea ice biomarker proxy  $IP_{25}$ , a related open-water highly branched isoprenoid (HBI) lipid (HBI III), and calcium carbonate ( $CaCO_3$ ) abundance related to carbonate chemistry and productivity/or preservation, were also analyzed. Over the last decade, source-specific highly branched isoprenoid (HBI) lipid biomarkers have emerged as reliable proxies for reconstructing past sea ice extent in the polar oceans (Belt, 2018 and references therein). The most frequently studied biomarker is the mono-unsaturated HBI  $IP_{25}$ , first identified in Arctic sea ice and sediments by Belt et al. (2007), and has since been used as a binary measure of seasonal Arctic sea ice in the past for time scales ranging from recent decades to several millions of years. Further, by combining sedimentary  $IP_{25}$  concentrations with those of various phytoplankton biomarkers in the form of the  $IP_{25}$ -phytoplankton ( $PIP_{25}$ ) index, semi-quantitative estimates of sea ice extent can be achieved (Belt, 2018; Müller et al., 2011). Finally, when a further tri-unsaturated HBI (often referred to as HBI III; Belt et al., 2015) is used as the open water counterpart to  $IP_{25}$ , the resulting  $PIP_{25}$  index (i.e.  $P_{III}IP_{25}$ ) exhibits a reasonably good linear relationship to spring sea ice concentration (%SpSIC) for the Barents Sea and neighboring regions (Smik et al., 2016).

North Atlantic and Arctic waters are characterized by distinct carbonate characteristics (e.g. alkalinity and pH), so carbonate abundance in sediments from the Fram Strait (mixing zone) can be used to infer changes in carbonate chemistry, productivity, preservation and dissolution resulting from variable paleo-oceanographic changes. For example, warm and carbonate-rich North Atlantic waters lead to better preservation compared to cold carbonate depleted Arctic waters. However, one of the

caveats attached with the application is the input of detrital carbonate to the core site. Study of carbonates in the core sites ODP 909 (Fram Strait) and 911 (Yermak Plateau) have suggested that predominant fractions of the carbonate abundance in the sediments are of authigenic origin and therefore controlled carbonate abundance variability in the Fram-Strait (Chow et al., 1996). Further, in previous studies, therefore, high carbonate preservation in sediments from the Fram Strait has been attributed to increased influence of Atlantic water masses (Zamelczyk et al., 2014). In the Norwegian–Greenland Sea, high carbonate content has also been interpreted to reflect the influence of warm Atlantic water masses, while low carbonate content were attributed to cold surface waters (Huber et al., 2000). Therefore, a combined authigenic Nd isotope and carbonate record from the Fram-Strait were employed in the present study to reconstruct northward volume and heat transport by the NAC.

## **2. Material and methods**

Sediments of ODP Hole 910C (80°15.894' N, 6°35.430' E; water depth: 556.4 m) have been analyzed in this study. The deep-water Nd isotope signal was extracted from the Fe-Mn oxyhydroxide fraction of bulk sediment following the leaching procedure described below. Further details of Nd isotopes, HBI biomarkers and calcium carbonate abundance measurements are given in the following sections.

### **2.1 Neodymium isotope analysis in authigenic fractions**

We measured the neodymium (Nd) isotope composition in authigenic phases extracted from the bulk sediments of 910C. This new record of authigenic  $\epsilon_{\text{Nd}}$  is supplemented by an earlier published low-resolution (60-70 ka) record from ODP Hole 911A at the



eastern flank of the Yermak Plateau (Teschner et al., 2016). Therefore, for comparison, and to avoid discrepancies related to the analytical methods for the extraction of authigenic Nd from sediments and its isotope measurements, we adopted the same method of Teschner et al. (2016). The procedure thus began with extracting the past seawater signal contained in the diagenetic coatings from ~2 g of sample material with a 0.05 M hydroxylamine hydrochloride and 15% acetic acid solution (HH leach), buffered to a pH of ~3.5 to 4.0, without rinsing before the HH leach. The rare earth elements (REEs) in the solution were separated using cation exchange columns filled with AG50WX8 resin (mesh 200–400). Nd was separated from the other REEs using columns filled with Ln-Spec resin (50–100 mesh). Nd isotopes were analyzed using a multi-collector inductively coupled plasma mass spectrometer (MC-ICP-MS, Thermo Scientific Neptune Plus) at the National Centre for Polar & Ocean Research (NCPOR), Goa, India. All Nd isotope ratios ( $^{143}\text{Nd}/^{144}\text{Nd}$ ) presented here were corrected for mass bias following an exponential law using the known value of  $^{146}\text{Nd}/^{144}\text{Nd}$  of 0.7219. The instrument bias was normalized to the accepted  $^{143}\text{Nd}/^{144}\text{Nd}$  value of the JNdi-1 standard of 0.512115 (Tanaka et al., 2000). Repeat measurements of the JNdi-1 standard yielded a long-term average reproducibility of  $\pm 0.3 \text{ } \epsilon_{\text{Nd}}$  ( $2\sigma$ ;  $n = 103$ ) over a period of nine months. Average procedural blank ascertained for Nd ( $n = 4$ ) was 170 pg which is less than 1% of the total Nd analyzed in samples, so blank correction was not applied. All Nd isotope ratios are reported in epsilon notation according to Equation 1.

$$\epsilon_{\text{Nd}} = \left[ \frac{^{143}\text{Nd}/^{144}\text{Nd}_{\text{sample}}}{^{143}\text{Nd}/^{144}\text{Nd}_{\text{CHUR}}} - 1 \right] \times 10^4 \quad \text{Eq (1)}$$

In order to check the quality of the authigenic Nd isotope analyses, which includes chemical extractions of the authigenic Nd and its isotopic measurements, we analyzed a

total of 16 replicates. Data from these replicates (with a variable range of  $\epsilon_{Nd}$ ) are highly consistent (Supplementary Fig. S1); most of them are falling on the equiline (1:1 line).

## 2.2 HBI biomarkers

The HBI biomarkers IP<sub>25</sub> and HBI III were extracted from freeze-dried subsamples (~2–4 g) from 910C. Samples were saponified in a methanolic KOH solution (~5 mL H<sub>2</sub>O: MeOH (1:9); 5% KOH) for 60 min (70 °C). Hexane (3×2 mL) was added to the saponified content, with supernatant solutions, containing non-saponifiable lipids (NSLs), transferred with glass pipettes to clean vials and dried over a gentle stream of N<sub>2</sub> to remove traces of H<sub>2</sub>O/MeOH. NSLs were then re-suspended in hexane (0.5 mL) and fractionated using column chromatography (SiO<sub>2</sub>; 0.5 g). Non-polar lipids, including IP<sub>25</sub> and HBI III, were eluted with hexane (6 mL). Each non-polar fraction was further purified to remove saturated components using silver-ion chromatography (Belt et al., 2015) with saturated compounds eluted with hexane (2 mL) and unsaturated compounds, including HBIs, collected in a subsequent acetone fraction (3 mL). Prior to extraction, samples were spiked with an internal standard (9-octylheptadec-8-ene, 9-OHD, 10  $\mu$ L; 10  $\mu$ g mL<sup>-1</sup>) to permit quantification of HBIs. Analysis of fractions containing IP<sub>25</sub> and HBI III was carried out using gas chromatography–mass spectrometry (GC–MS) following the methods and operating conditions described elsewhere (Belt et al., 2012). Mass spectrometric analysis was carried out in total ion current (TIC) and selected ion monitoring (SIM) modes. The identification of IP<sub>25</sub> and other HBIs was based on their characteristic GC retention indices (e.g. RI<sub>HP5MS</sub> = 2081 and 2044 for IP<sub>25</sub> and HBI III, respectively) and mass spectra (Belt, 2018). Quantification of all HBIs was achieved by comparison of mass spectral responses of

selected ions (e.g.  $IP_{25}$ ,  $m/z$  350; HBI III,  $m/z$  346) in SIM mode with those of the internal standard (9-OHD,  $m/z$  350) and normalized according to their respective instrumental response factors, derived from solutions of known biomarker concentration, and sediment masses (Belt et al., 2012).

Concentrations of  $IP_{25}$  and HBI III were combined in the form of the  $P_{III}IP_{25}$  index (Eq. 4), with the latter then used to provide semi-quantitative estimates of spring sea ice concentration (SpSIC (%), Eq. 5) according to a recent regional calibration (Smik et al., 2016). A root mean-square error of 11% associated with SpSIC estimates, was also calculated using regional calibration data (Köseoglu et al., 2018; Smik et al., 2016)

$$P_{III}P_{25} = \frac{IP_{25}}{(IP_{25} + (0.63 * HBI\ III))} \quad Eq\ (4)$$

$$SpSIC\ (\%) = \frac{(P_{III}IP_{25} - 0.0692)}{0.0107} \quad Eq\ (5)$$

Finally, we used the non-parametric CP3O algorithm from the R package ECP (R Core Team, 2018) to carry out change-point analysis on SpSIC estimates to identify significant shifts in the time series profile (Supplementary Fig. S2). All biomarker and %SpSIC data are provided in Supplementary Data 2.

### 2.3 Analysis of carbon

Analyses of total carbon (TC) and organic carbon ( $C_{org}$ ) were performed with a LECO SC-632 at the Geological Survey of Norway, Trondheim. For TC determination, subsamples of 300-400 mg were combusted at 1350°C and the release of  $CO_2$  was measured. For  $C_{org}$  analysis, sub-samples of 400-450 mg were placed in carbon-free pervious ceramic combustion boats. These were placed on a heating plate at 50°C ( $\pm$  5°C) and treated with 10 vol.% hydrochloric acid (HCl) to remove inorganic carbon

(carbonate) and subsequently rinsed with distilled water and dried in the drying oven prior to analysis. Carbonate content was calculated as  $\text{CaCO}_3 = (\text{TC} - \text{C}_{\text{org}}) \times 8.33$  with an assumption that calcite is the dominant form in the carbonate fraction (Vogt et al., 2001). Results are provided in weight percentage (wt. %) and the standard deviation of the TC and  $\text{C}_{\text{org}}$  measurements based on the repeated measurements of a standard was  $\pm 0.026$  wt% ( $1\sigma$ ,  $n=8$ ) and  $\pm 0.028$  wt. % ( $1\sigma$ ,  $n=11$ ), respectively.

#### **2.4 Age control for sediments deposited at ODP Hole 910C**

The age constraints for 910C is based on correlation of bio-stratigraphic and magneto-stratigraphic datums with Hole 911A together with additional benthic stable isotope data from 910C for the Pliocene (2.44 – 5.76 Ma). The age model based on the tie points and associated uncertainties have already been discussed in previous studies (Grøsfjeld et al., 2014; Knies et al., 2014b; Matningsdal et al., 2014). Briefly, five tie points formed the basis of the age model for our target interval between ~3.4 and 2.6 Ma in 910C (see Supplementary Table S1). Two tie-points at 190 mbsf and 305 mbsf inferred from seismic correlation between 910C and 911A mark the magneto-stratigraphic boundaries at 2.58 Ma (Matuyama/Gauss) and 3.6 Ma (Gauss/Gilbert) (Matningsdal et al., 2014). Support for this age model is provided by the biostratigraphic “Datum A” (~2.78 Ma) at ~223 mbsf in 910C (Sato and Kameo, 1996) and the glacial to interglacial oscillations of the benthic  $\delta^{18}\text{O}$  record of 910C (Knies et al., 2014a). Between “Datum A” (2.78 Ma) and the inferred Gauss/Gilbert boundary (3.6 Ma), we have originally applied an age model based on linear sedimentation rates between these two fix-points (Knies et al., 2014a). One major climate transition (i.e. MIS M2 glaciation) expressed by a sharp increase in the global  $\delta^{18}\text{O}$  stack (Lisiecki and Raymo,

2005) (Supplementary Fig. S4) falls within our targeted time interval of 3.4 to 2.6 Ma. We used the more radiogenic  $\epsilon_{\text{Nd}}$  peak at 260.4 mbsf in 910C as an additional tie point to define the MIS M2 glaciation (Supplementary Table S1, Supplementary Fig. S5), corresponding to a pronounced IRD pulse in Hole 911A (Supplementary Fig. S6). The calculated sedimentation rates between fix points either side of this new tie point are within the same order of magnitude (8 to 15 cm/ka) thus justifying this additional age fix point. The age of the “Datum A” corresponding to the depth 223 mbsf was constrained based on the occurrence of calcareous nanofossils in 910C and 911A (Sato and Kameo, 1996) and is slightly shifted from the original age of 2.78 Ma (Knies et al., 2014b) to 2.83 Ma in the revised age model (Supplementary Table S1). Together with the new tie points for biostratigraphic “Datum A” and shifted radiogenic  $\epsilon_{\text{Nd}}$  peak to MIS M2, we used the linear sedimentation rates between all tie points to establish the age model for 910C between 3.4 - 2.6 Ma (Supplementary Table S1). Based on the revised chronology, the most negative excursion in the authigenic  $\epsilon_{\text{Nd}}$  profile is now shifted from 2.981 to 3.081 Ma, while the most positive excursion defines the MIS M2 glaciation (Supplementary Fig. S4). Considering the uncertainty in our age model, it might be challenging to resolve all individual peaks and troughs corresponding to glacial-interglacial stages in our proxy records of authigenic  $\epsilon_{\text{Nd}}$ , biomarkers and  $\text{CaCO}_3$ ; however, the most prominent excursions in our proxy records during the mPWP can be resolved with confidence, which is the primary target interval of the present study. All information on previously published and new tie points are provided in Supplementary Table S1.

### 3. Results

#### 3.1 Authigenic $\epsilon_{\text{Nd}}$ record from the Yermak Plateau.

The new  $\epsilon_{\text{Nd}}$  record from the Yermak Plateau allows identification of the maximum limit of water mass exchange between the NAC and Arctic derived PW, particularly during the major climatic transitions of the Pliocene to the earliest Pleistocene (3.4–2.6 Ma). These include the MIS M2 glaciation (3.312–3.264 Ma), the mPWP (3.264–3.025 Ma) and the intensification of Northern Hemispheric glaciation (iNHG) at ~2.7 Ma ago. The authigenic  $\epsilon_{\text{Nd}}$  record shows long-term secular changes from -9.2 during the MIS M2 glacial period to -14.4 (5.2  $\epsilon_{\text{Nd}}$  unit) during the mPWP; the modern value of -11.7 reported (Lambelet et al., 2016) from the core site falling within this range. Thereafter, an increasing trend up to -7.8 at ~2.6 Ma is clearly discernable, with several prominent positive excursions associated with iNHG cold stages (Fig. 2c). Our  $\epsilon_{\text{Nd}}$  record for 910C exhibits a larger range (6.6  $\epsilon_{\text{Nd}}$  unit) compared to that of 911A (3.4  $\epsilon_{\text{Nd}}$  unit) (Teschner et al., 2016) within the time period 3.5 – 2.5 Ma (Fig. 2c), most likely due to the higher temporal resolution.

#### 3.2 Biomarker and $\text{CaCO}_3$ records.

The occurrence of seasonal sea ice throughout the record is confirmed by the near continuous presence of the biomarkers  $\text{IP}_{25}$  and HBI III (Fig. 2d). Although the concentration of HBI III is mainly lower than that of  $\text{IP}_{25}$ , it is the more abundant biomarker during the mPWP (ca. 3.150–2.970 Ma), consistent with more productive open-water conditions, as also shown by the carbonate record, which reaches its highest values during the MIS KM1-K2 (~3.150-3.050 Ma) (Fig. 2f). The  $\text{CaCO}_3$  abundance measured in the bulk sediments ranges from 0.5 to 6%; however, a sharp

three fold increase from the mean value  $\sim 2\%$  to  $6\%$  is evident during the mPWP, which coincides with the prominent negative excursion in the  $\epsilon_{Nd}$  record (Fig. 2c).

## 4. Discussion

The authigenic ferromanganese oxyhydroxide fraction extracted from the bulk sediments has been demonstrated to record the  $\epsilon_{Nd}$  signal of bottom waters of the Yermak Plateau (Teschner et al., 2016; Werner et al., 2014). Hence, temporal variations in authigenic  $\epsilon_{Nd}$  during glacial-interglacial periods have been primarily attributed to watermass exchange between the NAC and PW, changes in sediment provenance, and variable weathering input due to glacial erosion (Teschner et al., 2016). However, other factors/mechanisms that contributed to the past authigenic  $\epsilon_{Nd}$  variability are discussed in the following section.

### 4.1 Factors contributing to past authigenic $\epsilon_{Nd}$ variability

ODP Hole 910C is placed in the mixing zone between Atlantic- and Arctic-derived waters (Fig. 1) and is therefore well suited to monitor the relative influence of two water masses: (i) relatively warmer, high salinity water (i.e. the NAC characterized by a less radiogenic Nd isotope signature and (ii) relatively cold and less saline water (i.e. Arctic-derived PW) characterized by more radiogenic Nd isotopes. In the open ocean away from ocean margins and regions of deep-water formation, Nd appears to behave quasi-conservatively (Rempfer et al., 2011). Therefore, the variability in authigenic  $\epsilon_{Nd}$  record from the open ocean is mainly explained by the mixing of water masses with distinct  $\epsilon_{Nd}$  signatures (Lang et al., 2016). However, contributions from other sources of dissolved Nd can substantially influence the authigenic  $\epsilon_{Nd}$  record.

Assuming that the modern geological and tectonic setting of the study region have largely remained stable over the past ~4.6 Ma (Knies et al., 2014a), we discuss the following potential mechanisms and factors that may have contributed to the variability and changes in the authigenic  $\epsilon_{Nd}$  record of 910C: (i) changes in weathering regimes and sediment sources; (ii) boundary exchange processes; and (iii) volumetric exchange of the NAC and PW.

Dissolved radiogenic isotope signatures in seawater originate from weathering processes of the continental crust (Frank, 2002) and, therefore, the glacial-interglacial changes in chemical weathering could influence the  $\epsilon_{Nd}$  record. Teschner et al. (2016) reconstructed past water mass mixing and erosional inputs prior and post intensification of Northern Hemisphere glaciation (iNHG, ~2.7 million years ago) based on records of radiogenic isotopes of Sr, Nd and Pb at ODP Hole 911A. Changes in the authigenic  $\epsilon_{Nd}$  record were highlighted for two different scenarios; (i) prior to the iNHG, the Pb and Nd isotopes composition was characterized by unradiogenic values and low variability due to the limited extent of ice sheets. These observations are consistent with earlier inferences from the Arctic Ocean (Haley et al., 2007) and suggest constant erosional supply of material to the Yermak Plateau, most likely from local sources (i.e. Svalbard). (ii) After the iNHG, conditions changed dramatically with higher-amplitude  $\epsilon_{Nd}$  variability in both deep waters and detrital sediments inputs due to changes in weathering inputs associated with the waxing and waning of the Eurasian ice sheets, water mass exchange and increased supply of ice-rafted debris (IRD). Comparison of the IRD record (Knies et al., 2014b) with our  $\epsilon_{Nd}$  record, shows higher IRD flux during the periods of MIS M2 glaciation and iNHG (~2.7 Ma), and low and stable IRD fluxes during



the mPWP (Supplementary Fig. S6). The latter corresponds to the IRD record from Site U1307 on Eirik Drift where coarse IRD is largely absent during the mPWP, and IRD is only present in small abundances during (de)glacials between ~3 Ma and 2.75 Ma. Therefore, higher variability in IRD supply and change of its sources could influence the authigenic  $\epsilon_{\text{Nd}}$  record in 910C; however, this can be excluded for the interglacial periods prior to the iNHG, particularly during the mPWP. It is also important to note that the timing of the iNHGs was further shifted to post MIS G2 (2.64 Ma) based on the Pb isotope and geochemical studies of the IRD on the lower eastern flank of the Reykjanes Ridge (Bailey et al., 2013). Therefore, we suggest that the observed variability and changes in the radiogenic Nd isotope record in 910C is affected by glacial weathering input probably during the MIS M2 glaciation and after the iNHG. In contrast, it is unlikely to be significantly affected by the changes in chemical weathering inputs and/sediment transport from distant sources during our targeted time interval of mPWP due to the stability of the climatic conditions and glacial erosion was rather limited.

The chemical weathering of Iceland-derived basaltic material can influence the Nd isotope composition of the NAC resulting in a shift towards more radiogenic values. However, in an earlier study, it has been suggested that present day exchange with Iceland derived basaltic material does not affect the deep water  $\epsilon_{\text{Nd}}$  signature of the main path of North Atlantic inflow, although it can influence the signature of southward flowing currents such as the East Greenland Current (Chen et al., 2012; Lacan and Jeandel, 2004).

Seawater interactions with the continental margins (boundary exchange) could be a potential source for radiogenic isotope signatures of seawater, particularly in the

Nordic Seas where basaltic formations are highly susceptible to dissolution and exchange with seawater (Chen et al., 2012; Lacan and Jeandel, 2004). The effects of boundary exchange have been reported from different continental margins in the subpolar regions including the Nordic Seas, and model results confirmed the importance of this input mechanism (Rempfer et al., 2011). Due to the large shelf areas of the Arctic Ocean, boundary exchange might be expected to be significant, although the water column data available so far do not provide clear evidence for this process (Andersson et al., 2008). Further, Laupkert et al (2017) suggested recently that  $\epsilon_{Nd}$  values around -10 are present in the eastern and western Fram Strait below ~500 m, implying that there is no evidence for boundary exchange processes influencing the  $\epsilon_{Nd}$  record to a significant extent on the Yermak Plateau.

In summary, with the absence of any significant ice-rafting prior to ~2.7 Ma (except MIS M2) in the Nordic Seas (Fig. 2e), increased sea surface temperatures (SST) by 3–7°C (Lawrence et al., 2009) between 3.4 and 2.6 Ma compared to the Holocene mean annual SST (Fig. 2g; dashed line) (Calvo et al., 2002), and thus no widespread Northern Hemisphere glacial advances, we attribute the large range in  $\epsilon_{Nd}$  (-14.8 to -9.0) in 910C prior to the iNHG to changes in watermass circulation rather than to variable glacial weathering input. As such, the prominent negative excursion in the  $\epsilon_{Nd}$  record during the mPWP (i.e. -14.4  $\epsilon_{Nd}$  units; Fig. 2c) is most likely due to an increase in volume transport of the NAC, resulting in an Atlantic-dominated climate regime of the Eurasian sector of the Arctic Ocean. Further, the prominent negative excursion in  $\epsilon_{Nd}$  record coincides with a sharp three-fold increase in  $CaCO_3$  abundance during the mPWP (Fig. 2f). This suggests an increased flow of warm NAC with higher

pH resulted in better preservation of carbonate and/or increase in productivity during interglacial periods in the eastern Fram Strait (Supplementary Figs. S7b, d, e), consistent with earlier reports from modern and Quaternary sediments (Huber et al., 2000).

To test the hypothesis of increased “Atlantification” and its concurrent sea ice decline further, we quantified the volumetric changes of the AW-derived water masses and sea ice concentration at 910C using (1) a simplified binary mixing model by constraining the end member values of  $\epsilon_{Nd}$  for two water masses and (2) semi-quantitative estimates of spring sea ice concentration (%SpSIC) based on a regional calibration of biomarker distributions in modern sediments (Smik et al., 2016).

#### 4.2 Quantifying water mass exchange based on authigenic $\epsilon_{Nd}$ record

Compilation and reassessment of seawater Nd data from the literature shows that the characteristic NAC  $\epsilon_{Nd}$  signature near its origin in the inter-gyre region (north of 46° N) displays  $\epsilon_{Nd}$  values between  $-14.0 \pm 0.3$  and  $-15.1 \pm 0.3$  (Dubois-Dauphin et al., 2017), which changes gradually during transport across the Arctic Mediterranean due to mixing of more radiogenic signatures of PW ( $\epsilon_{Nd} = -9.9 \pm 0.7$ , 1 SD (standard deviation) and  $[Nd] = 27.1$ ) (Laukert et al., 2017). We have assigned  $\epsilon_{Nd}$  and  $[Nd]$  values for the NAC ( $-15 \pm 1$  (1 SD) and  $16 \pm 1$  pmol/kg) and PW ( $-9.9 \pm 1$  (1 SD) and  $27 \pm 1$  pmol/kg) end-members, respectively, which are clearly distinct from the modern value in the Fram Strait (mean  $\epsilon_{Nd} = -11.7 \pm 0.8$  (2SD)) (Laukert et al., 2017). With this identification of suitable end-member values for  $\epsilon_{Nd}$ , we therefore adopt a simple binary mixing approach for the determination of the percentage Atlantic water component (%AWC) on the assumption that Nd behaves quasi-conservatively and end-member compositions

were invariant during the studied time interval. Such assumptions are discussed in more detail in the Supplementary Note 2. Meanwhile, we note that this method was successfully employed in a previous study (Lang et al., 2016) using a Nd isotope record from the late Pliocene (3.3–2.4 Ma ago) to quantify the mixing proportion of southern source water and north Atlantic deep water (NADW) in the North Atlantic.

#### 4.2.1 Binary estimates of Atlantic water mass mixing using authigenic $\epsilon_{Nd}$ record

We have used the  $\epsilon_{Nd}$  record from 910C to generate the semi-quantitative estimate of water-mass mixing between NAC and PW during the Late Pliocene to early Pleistocene (~3.4 - 2.6 Ma). The underlying assumptions of this approach are: (i) Nd isotopes exhibit quasi-conservative behaviour, (ii) mixing of Atlantic- and Arctic-derived waters at 910C is binary, and (iii) modern day end-members have been invariant between 3.4 and 2.6 Ma. We used the following binary mixing equation constrained by our current understanding of end-member compositions:

$$\epsilon_{Nd_{910C}} = \frac{\epsilon_{Nd_{AW}} * C_{AW} * f_{AW} + \epsilon_{Nd_P} * C_{PW} * f_{PW}}{C_{AW} * f_{AW} + C_{PW} * f_{PW}} \quad Eq (2)$$

$$f_{AW} + f_{PW} = 1 \quad Eq (3)$$

where  $\%AWC_{\epsilon_{Nd}} = f_{AW} * 100$  is the relative contribution of Atlantic water component to 910C ( $\%PWC_{\epsilon_{Nd}} = 100 - \%AWC_{\epsilon_{Nd}}$ ),  $C_{PW}$  and  $C_{AW}$  represent the concentration of Nd in the Arctic (PW) and the Atlantic (AW),  $\epsilon_{Nd910C}$  is the value of Nd isotope compositions of sediment leach from 910C, and  $\epsilon_{AW}$  and  $\epsilon_{PW}$  are the end-members of isotope composition of Atlantic and Arctic water masses, respectively.  $f_{AW}$  and  $f_{PW}$  represent the fractions of Nd coming from the Atlantic (AW) and Arctic (PW) waters.

In order to validate the use of this binary mixing model to 910C, we also calibrated our approach by comparison of semi-quantitative estimates of modern day volume transport with in situ observations. We thus estimated the modern day volume transport of NAC using a contemporary  $\epsilon_{Nd}$  value at the borehole site of 910C and compared that with a mooring-based observation (Beszczynska-Moeller et al., 2012). Our estimate of %NAC based on  $\epsilon_{Nd}$  ( $47 \pm 9\%$ ) (Supplementary Fig. S9) compares well with a value of  $45 \pm 5\%$  (Supplementary Fig. S9b) measured from an array of moorings in Fram Strait ( $78^\circ 50' N$ ) over the period 1997–2010 (Beszczynska-Moeller et al., 2012).

We have determined the uncertainty associated fractions of NAC volume estimates using a Monte-Carlo error propagation method with 10,000 iterations in MATLAB, which is represented as an error envelop (at 95% confidence) (Fig. 3a). However, we offer some caution that our %NAC estimates may be subject to changes in the future when more suitable archives allow generation of orbital resolution records of NAC and PW end-member behaviour. For now, the uncertainties reported here for our  $\epsilon_{Nd}$ -based estimates of %NAC may be underestimated due to limited knowledge of end-member  $\epsilon_{Nd}$  values for Atlantic and Arctic waters. On the other hand, our main conclusions over our targeted time interval (3.4 – 2.6 Ma) are not influenced by such uncertainties.

Our estimates of %AWC in 910C indicate three distinct peaks with values close to 100%, indicating the presence of a dominant Atlantic watermass in the water column during the three interglacial events (Haywood et al., 2013) (i.e. MIS KM3, K1, and G17) within or close to the mPWP; albeit within the limitation of the age constraints of 910C

(Fig. 3 a). For MIS KM5c, with near-modern orbital configuration, the %AWC ( $51 \pm 11\%$ ) was similar to today ( $45 \pm 5\%$ ) (Beszczynska-Moeller et al., 2012; Zhang et al., 2013) but was close to  $\sim 0\%$  during the preceding MIS M2 glaciation (3.305–3.285 Ma) (Fig. 3a), consistent with previous observations of a weaker NAC and concurrent cooling in the circum-Arctic (De Schepper et al., 2015). Importantly, although %AWC estimates for the glacial periods (i.e. MIS M2 and iNHGs) might potentially suffer higher uncertainty due to enhanced IRD flux and weathering inputs associated with higher glacial activity, such effects during the mPWP are likely insignificant, in practice, due to the relatively stable climate and lower IRD fluxes (Blake-Mizen et al., 2019; Knies et al., 2014a) (Fig. 2e and Supplementary Fig. S6). Pertinent to our reconstructed reduced flux of %AWC during the MIS M2 glaciation, we note that a similar situation has been reported for MIS6 based on authigenic coupled isotope records of Nd and Hf from the central Arctic Ocean (Chen et al., 2012).

## **4.2 Sea ice reconstruction**

Extensive sea ice cover ( $>60\%$  SpSIC) prevailed from 3.36–3.18 Ma, including maximum extent during MIS M2 (Fig. 3b). Thereafter, %SpSIC reduced substantially. According to Smik et al. (2016), biomarker-based %SpSIC estimates above ca. 68% also imply the occurrence of some summer sea ice ( $>5\%$  summer sea ice concentration (SuSIC)) (Supplementary Fig. S3). Similarly, while the occurrence of some summer sea ice was a common feature up to ca. 3.18 Ma (Fig. 3b), coincident with consistently low %AWC (i.e. below the modern value of 45%; Fig. 3a), ice-free summers were likely a common feature at the Yermak Plateau thereafter, especially during the mPWP. Change-point analysis carried out on our %SpSIC estimates shows

a statistically significant decrease of ca. 30–35% starting at ca. 3.15 Ma before increasing again at ca. 2.97 Ma (Supplementary Fig. S2). Prior to this, extensive sea ice cover similar to the modern (spring) maximum prevailed, including maximum extent during MIS M2 when the %AWC was at a minimum (Fig. 3a, b). The reduction in SpSIC during the mPWP likely reflects a response to increased %AWC, analogous to observations made for eastern Fram Strait (Spielhagen et al., 2011) and the Barents Sea spanning recent decades/centuries (Cabedo-Sanz and Belt, 2016). Similar observations have been reported for the Early Holocene and the Last Interglacial (MIS5e/Eemian), implying that increased Atlantic Water inflow is one important factor controlling sea ice conditions in an area covering northern Svalbard/Yermak Plateau and the northern Barents Sea continental margin (Belt et al., 2015; Müller et al., 2012; Stein et al., 2017). According to our SpSIC estimates, maximum sea ice extent during the mPWP exhibited a closer resemblance to that of modern-day late summer (i.e. minimum) conditions (Fig. 3b). These new data support the boundary conditions used in the Pliocene Research, Interpretation and Synoptic Mapping (PRISM) project, which assumes a conservative sea ice extent, an ice-free Arctic Ocean in summer, and winter sea ice conditions approximately equivalent to modern summer ice extent (Dowsett et al., 2010).

#### **4.3 Forcing factors modulating North Atlantic volume transport and its impact**

Our new reconstructions of watermass mixing and carbonate abundances follow the periodicities of eccentricity (~100 ka), obliquity (~40) and precessional cycles (~20 ka) (Figs. 4a, b). Further, the %AWC and %SpSIC records show good alignment with the eccentricity (Fig. 4c) and summer insolation in the northern hemisphere (Fig. 5b),

implying orbitally-paced control over changes to oceanic heat flow into the Arctic Ocean. Cross wavelet analysis highlights the common highest power between these two time series in colour bands (Fig. 4c). The vector arrows indicate an in-phase relation (pointing rightward) during 3.2 – 2.9 Ma at the eccentricity band (64 – 128 ka), implying that orbitally-controlled, enhanced NAC contribution resulted in an increase in marine productivity and reduction in sea ice coverage during the mPWP (Supplementary Fig. S7c, d). In particular, during the three interglacials with high eccentricity (i.e. KM3, K1, and G17; Fig. 5a, d), increased seasonality combined with warmer summers (higher solar insolation) in the Northern Hemisphere (Fig. 5a, b) may have resulted in an increased oceanic heat transport with consequential decline in Arctic sea ice extent and polar amplification of this warming. Alternatively, an orbitally-forced reduction in Arctic sea ice coverage may have changed buoyancy and salinity in the Atlantic, and thus been responsible for increased northward ocean heat transport during mPWP interglacials leading to a strongly positive ice-albedo feedback. Our proxy data do not reveal any correspondence with variable atmospheric CO<sub>2</sub> estimates (Fig. 5c, d and e) implying only a minor influence of greenhouse gas-derived radiative forcing in modulating NAC heat transport and reduction in Arctic sea ice. Further, tectonic changes could have driven circulation changes as has been reported for the Bering Strait and Nordic Sea related to reconfiguration of oceanic gateways (De Schepper et al., 2015; Horikawa et al., 2015). However, the strong signal of orbital cycles in our proxy records clearly indicate that the orbital forcing played the dominant role over all other controlling factors.



Based on multi-proxy records, it has been inferred that the Atlantic Meridional Overturning Circulation (AMOC) was significantly stronger in the mPWP compared to today (Raymo et al., 1996; Frank et al., 2002; Dowsett et al., 2009), which could have contributed to enhanced northward heat transport during the mPWP interglacials (Dowsett et al., 2009; Lawrence et al., 2010; Naafs et al., 2012), consistent with our findings. However, the exact mechanism(s) responsible for changes in northward heat transport remain a topic of debate (Haywood et al., 2016; Haywood et al., 2013; Zhang et al., 2013), but could potentially be resolved through further ocean modelling studies that integrate the new proxy data presented herein.

Regardless of the ultimate driver(s), our estimates of %AWC show a clear dominance of a warm and well-mixed Atlantic-dominated climate regime in the Eurasian Arctic during MIS KM3, K1, and (within the given age uncertainties) G17, with lower than modern sea ice extent (including ice-free summers) and higher marine productivity, consistent with modeled and reconstructed amplification of Arctic surface temperatures (Ballantyne et al., 2013), and a rise in annual mean surface air temperatures between 4°C to 5°C ( $\Delta t = \text{Plio-KM5c} - \text{pre-industrial}$ ) (Prescott et al., 2018). This implies that the increase in %AWC with concurrent reduction in %SpSIC during these mPWP interglacials resembles modern observations of an advanced “Atlantification” of the study region (Cabedo-Sanz and Belt, 2016; Naafs et al., 2010; Spielhagen et al., 2011).

The conclusion of increased “Atlantification” of the Arctic during the mPWP from our new proxy records from the Atlantic-Arctic gateway confirms previous studies from lower latitudes a (Naafs et al., 2010; Raymo et al., 1996). Since current generation models have not yet been validated against any proxy-based observations of

“Atlantification” in the Eurasian sector of the Arctic during the mPWP, our new Nd isotope, biomarker and  $\text{CaCO}_3$  records thus provide important input for testing the robustness of future climate modelling for northern high latitude settings.

## **5. Conclusions**

Our new Nd isotope record of past water mass exchange in the Atlantic-Arctic gateway relative to the modern-day setting suggests a near doubling of NAC volume transport during mPWP interglacials KM3, K1, and G17 with different orbital configurations and thus stronger seasonality than today. This resulted in a warm and well-mixed Atlantic-dominated climate regime (“Atlantification”) of the Eurasian sector of the Arctic Ocean, reduced spring sea ice concentration, and the possibility of ice-free conditions during summers. In contrast, the mPWP interglacial with near-modern orbits (MIS KM5c) does not show significant deviation from today’s NAC volume transport or sea ice extent. This study demonstrates a dominant role of orbital forcing in modulating northward ocean heat transport and Arctic sea ice coverage during the mPWP. It also highlights the importance of improving data-model comparison studies for the Arctic Ocean that integrate reconstructions of water mass flow and ocean circulation, as well as temperature and sea ice, for climate states of the past that may be analogous to the future.

### **Data availability**

All the data are provided in the supplementary and also will be archived in PANGAEA upon acceptance of the manuscript.

### **Code availability**

The MATLAB codes for uncertainty estimates on the volumetric water fractions of Atlantic water are available from the corresponding author W. Rahaman on request.

## **Acknowledgements**

We acknowledge Ministry of Earth Sciences, Govt. of India, NCPOR, and Research Council of Norway through its funding scheme for CAGE (223259) and PACT (248793). We thank Manish Tiwari for his support as a Co-PI in the PACT project. We thank C Torrence, GP Compo, A Grinsted, JC Moore, and S Jevrejeva for MATLAB codes. Authors thank Priya Lokhande for initial handling of the sample for Nd isotope chemistry and Rohit Srivastava for providing MATLAB codes for Monte-Carlo error propagation. We thank two anonymous reviewers who provided supportive and constructive feedback on the initial version of this manuscript. Finally, we thank Laura F Robinson for editorial handling of the manuscript.

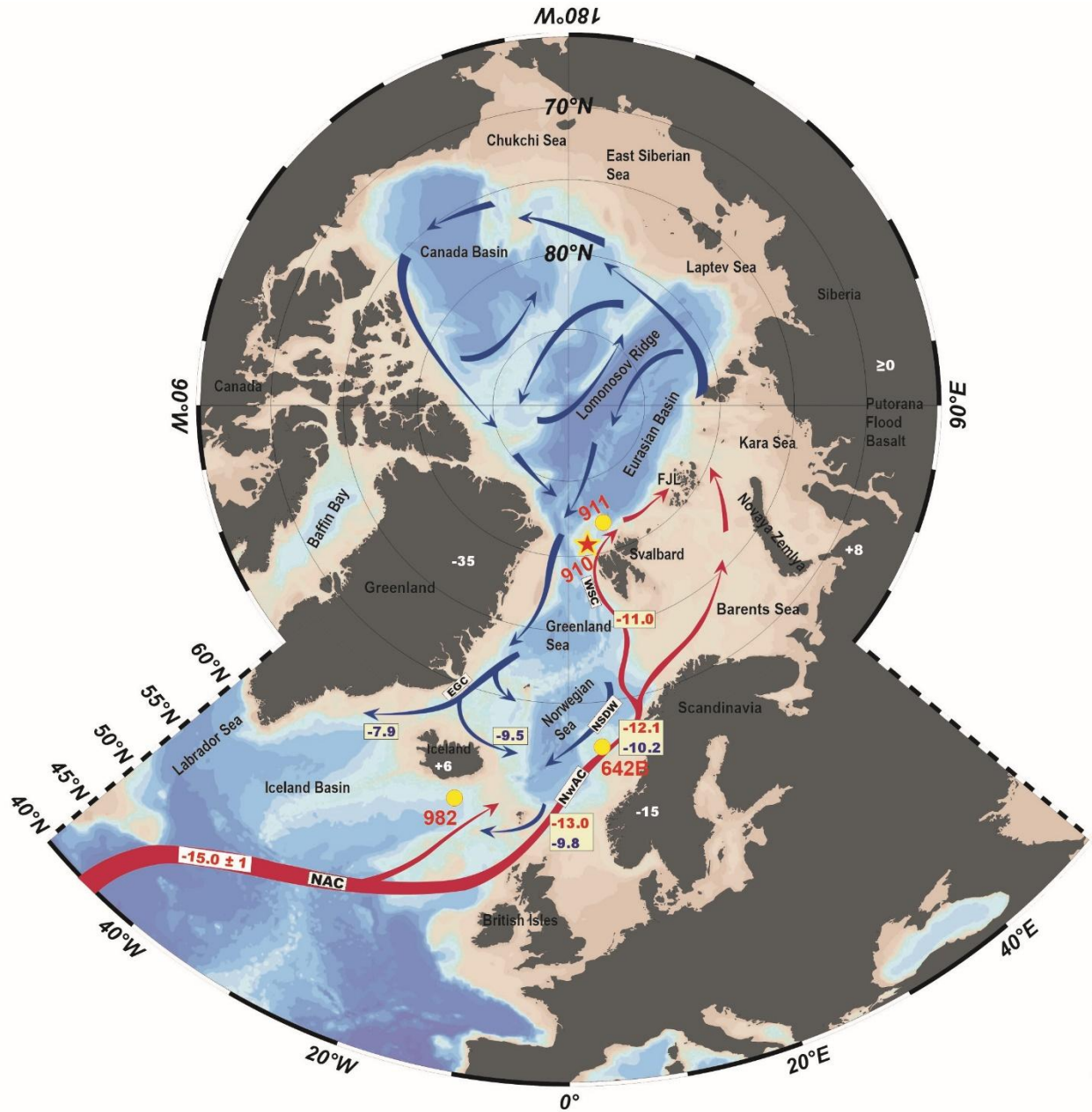
## **Author contributions**

W.R., J.K. and M.T. designed the study. W.R., J.K., S.T.B and A.H wrote most of the text. Analysis of model results was completed by A.H and J.T. Mo.T. and L.N. analyzed authigenic Nd isotope compositions in bulk sediment. L.S, D.K and S.T.B. measured the concentrations of the  $IP_{25}$  and HBI III biomarkers in bulk sediments and interpreted outcomes. All authors contributed to interpreting results, discussion and improvement of this paper.

## **Competing interests**

The authors declare no competing interests.

587



588

589 **Fig. 1. Water mass circulation and their characteristic Nd isotope compositions.** Locations of ODP  
 590 Sites 910 (red star) and 911 (filled yellow circle) with schematic flow paths of the main water masses in  
 591 the northern North Atlantic and Nordic Seas and their present-day  $\epsilon_{Nd}$  signatures (Teschner et al., 2016).  
 592 Dark red arrows mark the warm inflowing Atlantic water; dark blue arrows represent the cold deep and  
 593 surface water masses flowing out of the Arctic Ocean (Andersson et al., 2008; François and Catherine,

594 2004; Lacan and Jeandel, 2004). White numbers mark the average  $\epsilon_{Nd}$  values of the bedrocks of  
595 Svalbard(Tütken et al., 2002), the Norwegian Caledonian Margin and Iceland(Laskar et al., 2004), the  
596 Putorana basalts in Russia (Sharma et al., 1992), and Greenland (François and Catherine, 2004).  
597 Positions of ODP site 982 (58° N, 16° W) and ODP Hole 642B (67° 20' N, 2° 90' E) are shown.

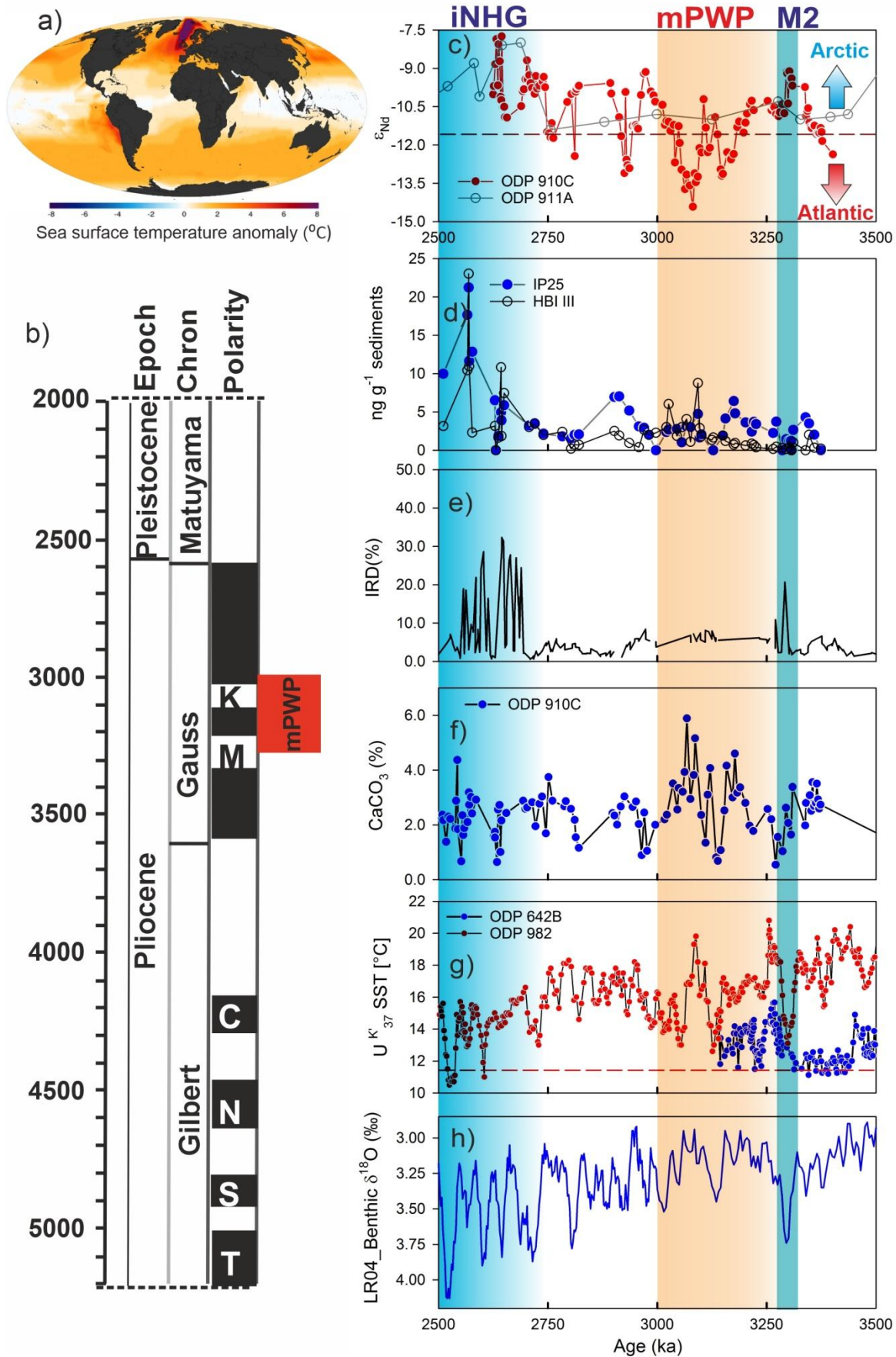


**Fig. 2. Water mass exchange and associated changes in the Fram Strait during the Late-Pliocene and Pleistocene** (a) Sea surface temperature (SST) anomalies during the mPWP (~3.3 – 3.0 Ma) compared to today (Dowsett et al., 2009). b) Pliocene-Pleistocene time scale with paleo-magnetic reversals. Red block represents the time slice of mPWP. c) Authigenic  $\epsilon_{Nd}$  record from 910C (this study) and 911A (Teschner et al., 2016). d) Record of sea ice and open water biomarkers IP<sub>25</sub> and HBI III. (e) Record of IRD (%) from ODP site 911A (Knies et al., 2014b). f) Record of CaCO<sub>3</sub> abundance (wt. %). g) Record of alkenon UK<sub>37</sub> derived SST at ODP Sites 982(Lawrence et al., 2009) (58° N, 16° W) and ODP Hole 642B(Bachem et al., 2017) (67° 20' N, 2° 90' E). Dashed lines indicate Holocene average SSTs for the Norwegian Sea(Calvo et al., 2002) at 11.6 °C. h) Benthic  $\delta^{18}O$  (LR04) stack(Lisiecki and Raymo, 2005). The shaded bands represent the major climatic transitions: M2 glaciation (blue shade, 3.312–3.264 Ma), mid-Pliocene Warm Period (mPWP) (brown shade, 3.3–3.0 Ma) and intensification Northern Hemisphere glaciation (iNHG, ~2.7 Ma).



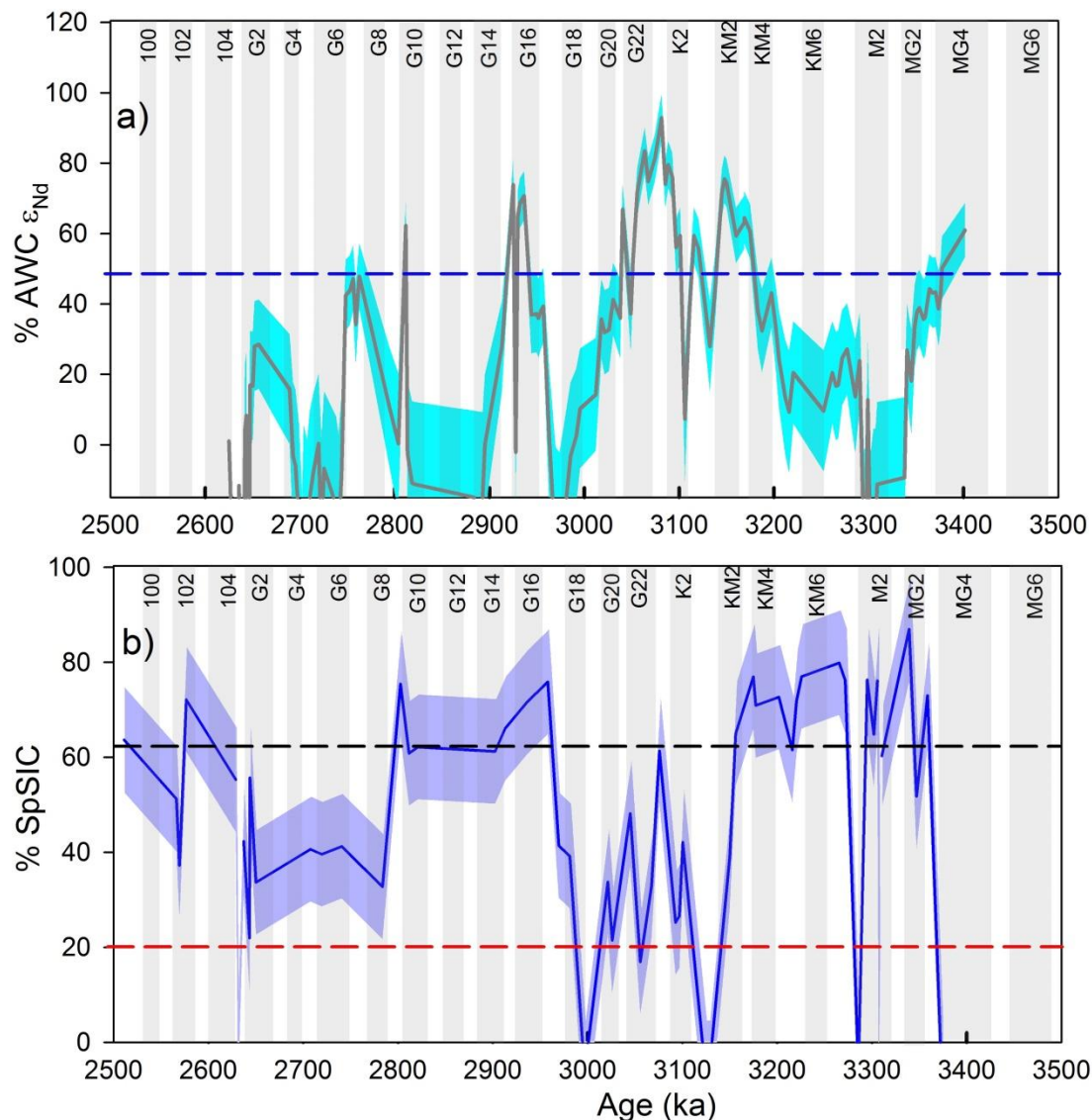
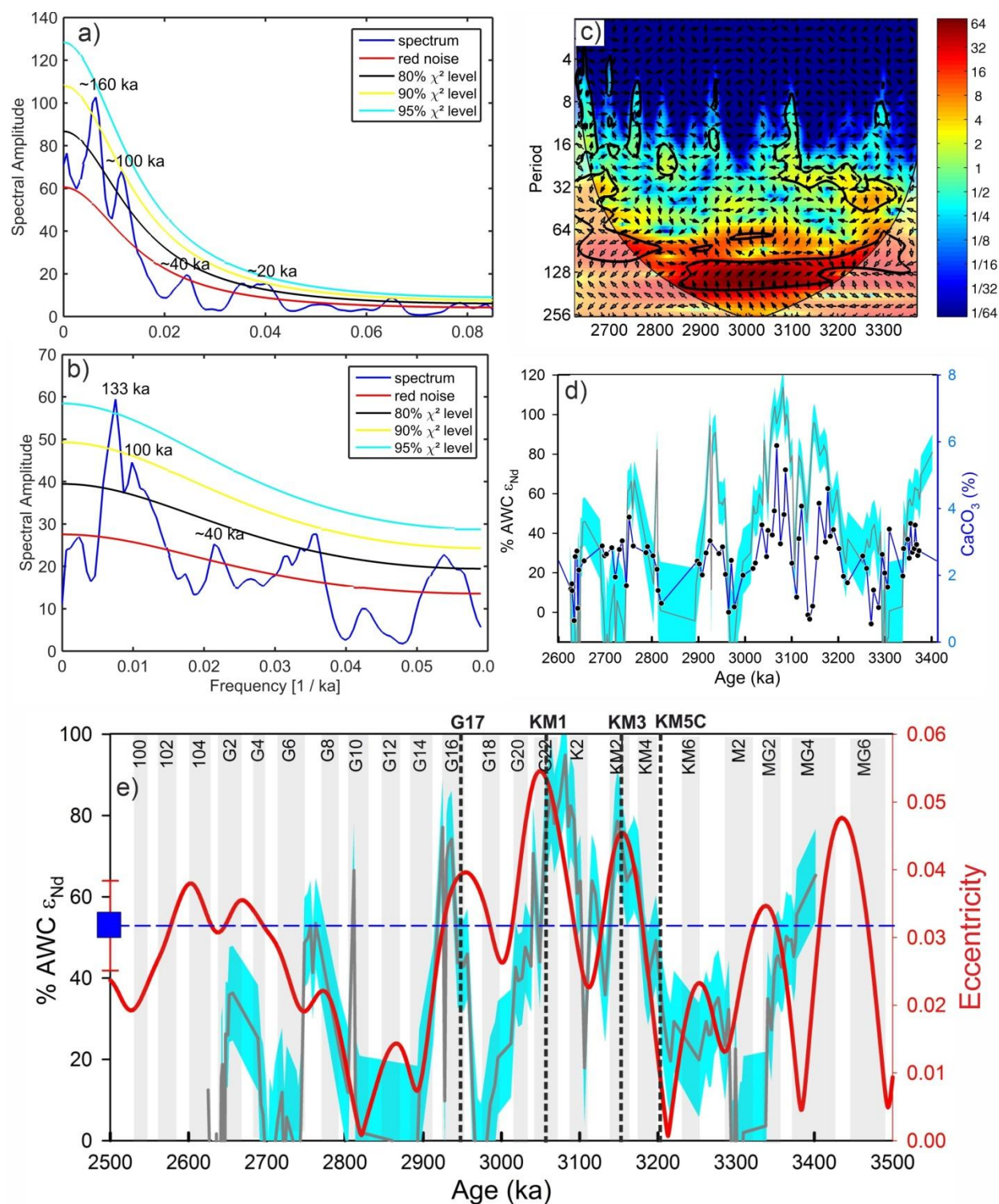


**Fig. 3. North Atlantic (NAC) volume transport and corresponding Arctic Sea Ice changes.** a) Fraction of Atlantic Water Component (%AWC<sub>εNd</sub>). Dark gray line: Best estimate. Shading: 95% confidence interval. Blue dashed line indicates modern Atlantic flow based on mooring estimate (Beszczynska-Moeller et al., 2012). (b) Spring sea ice (%). Solid blue line represents mean value. Blue shade represents root-mean-square error (RMSE) on the mean value. Blue and red dashed horizontal lines represent the modern mean (1988-2017, NSIDC) sea ice maximum (62%, Apr-June; spring) and minimum (20%, September; late summer) concentrations at the core site.



630



631

632 **Fig. 4. Identification of orbital cycles in proxy records.** Power spectrum analysis of (a) NAC volume  
633 transport and (b)  $\text{CaCO}_3$  abundance (%) records from the Yermak Plateau. They show periodicities of

634 orbital cycles at different significance level. c) Cross wavelet analysis of two time series highlights the  
635 common highest power between these two time series which is highlighted in color code. Vector arrow  
636 indicates phase relation between the time series. The 5% significance level against red noise is shown as  
637 a thick contour. The thin solid line indicates cone of influence. The relative phase relationship is shown as  
638 arrows (with in-phase pointing right, anti-phase pointing left, and  $\epsilon_{Nd}$  leading  $CaCO_3$  by  $90^\circ$  pointing  
639 straight down and vice versa). d) Comparison of the record of NAC with  $CaCO_3$  percentage, an indicator  
640 of marine productivity. Both the curves overall follow the same pattern; the highest abundance in calcium  
641 carbonate and thus the highest productivity was observed during mPWP when NAC flow was maximum.

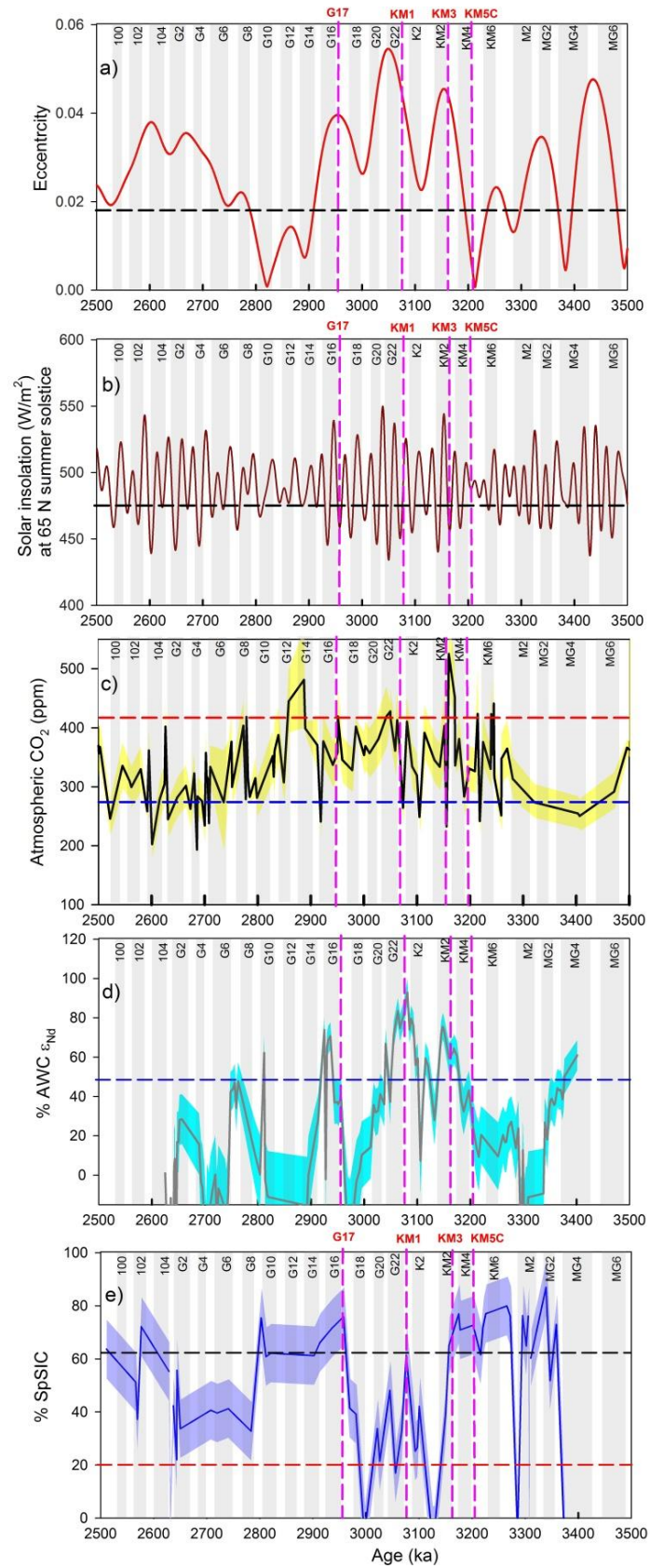


**Fig. 5 Role of orbital forcing in modulating watermass exchange and spring sea ice extent.** (a) Record of eccentricity (Laskar et al., 2004). Dashed horizontal line represents modern eccentricity. Vertical dashed lines (pink) indicate four interglacial periods KM5C, KM3, KM1 and G17. Among these four interglacial periods, KM5C is most similar to that of the modern orbital forcing (Haywood and Valdes, 2004). (b) Record of solar insolation at 60° N summer solstice (Laskar et al., 2004). Dashed line represents modern value of summer insolation. c) Record of atmospheric pCO<sub>2</sub> derived from boron isotopes ( $\delta^{11}\text{B}$ ) (Foster et al., 2017). Yellow band represents error envelopes (1 $\sigma$  SD). Black and red colour dashed lines represent pre-industrial CO<sub>2</sub> (280 ppm) and present CO<sub>2</sub> (~410 ppm) level. These forcing parameters are compared with fraction of d) Atlantic Water (%AWC) and (e) Spring sea ice (%).

## References

- Andersson, P.S., Porcelli, D., Frank, M., Björk, G., Dahlqvist, R., Gustafsson, Ö., 2008. Neodymium isotopes in seawater from the Barents Sea and Fram Strait Arctic–Atlantic gateways. *Geochimica et Cosmochimica Acta* 72, 2854-2867.
- Bachem, P.E., Risebrobakken, B., De Schepper, S., McClymont, E.L., 2017. Highly variable Pliocene sea surface conditions in the Norwegian Sea. *Clim. Past* 13, 1153-1168.
- Bailey, I., Hole, G.M., Foster, G.L., Wilson, P.A., Storey, C.D., Trueman, C.N., Raymo, M.E., 2013. An alternative suggestion for the Pliocene onset of major northern hemisphere glaciation based on the geochemical provenance of North Atlantic Ocean ice-rafted debris. *Quaternary Science Reviews* 75, 181-194.
- Ballantyne, A.P., Axford, Y., Miller, G.H., Otto-Bliesner, B.L., Rosenbloom, N., White, J.W.C., 2013. The amplification of Arctic terrestrial surface temperatures by reduced sea-ice extent during the Pliocene. *Palaeogeography, Palaeoclimatology, Palaeoecology* 386, 59-67.
- Belt, S.T., 2018. Source-specific biomarkers as proxies for Arctic and Antarctic sea ice. *Organic Geochemistry* 125, 277-298.
- Belt, S.T., Brown, T.A., Rodriguez, A.N., Sanz, P.C., Tonkin, A., Ingle, R., 2012. A reproducible method for the extraction, identification and quantification of the Arctic sea ice proxy IP25 from marine sediments. *Analytical Methods* 4, 705-713.
- Belt, S.T., Cabedo-Sanz, P., Smik, L., Navarro-Rodriguez, A., Berben, S.M.P., Knies, J., Husum, K., 2015. Identification of paleo Arctic winter sea ice limits and the

687 marginal ice zone: Optimised biomarker-based reconstructions of late  
688 Quaternary Arctic sea ice. *Earth and Planetary Science Letters* 431, 127-139.

689 Berends, C.J., de Boer, B., Dolan, A.M., Hill, D.J., van de Wal, R.S.W., 2019. Modelling  
690 ice sheet evolution and atmospheric CO<sub>2</sub> during the Late Pliocene. *Clim. Past*  
691 15, 1603-1619.

692 Beszczynska-Moeller, A., Fahrbach, E., Schauer, U., Hansen, E., 2012. Variability in  
693 Atlantic water temperature and transport at the entrance to the Arctic Ocean,  
694 1997-2010.

695 Blake-Mizen, K., Hatfield, R.G., Stoner, J.S., Carlson, A.E., Xuan, C., Walczak, M.,  
696 Lawrence, K.T., Channell, J.E.T., Bailey, I., 2019. Southern Greenland glaciation  
697 and Western Boundary Undercurrent evolution recorded on Eirik Drift during the  
698 late Pliocene intensification of Northern Hemisphere glaciation. *Quaternary*  
699 *Science Reviews* 209, 40-51.

700 Cabedo-Sanz, P., Belt, S.T., 2016. Seasonal sea ice variability in eastern Fram Strait  
701 over the last 2000 years. *arktos* 2, 22.

702 Calvo, E., Grimalt, J., Jansen, E., 2002. High resolution U37K sea surface temperature  
703 reconstruction in the Norwegian Sea during the Holocene. *Quaternary Science*  
704 *Reviews* 21, 1385-1394.

705 Chen, T.-Y., Frank, M., Haley, B.A., Gutjahr, M., Spielhagen, R.F., 2012. Variations of  
706 North Atlantic inflow to the central Arctic Ocean over the last 14 million years  
707 inferred from hafnium and neodymium isotopes. *Earth and Planetary Science*  
708 *Letters* 353-354, 82-92.



- 709 Chow, N., Morad, S., Al-Aasm, I., 1996. Origin of Authigenic Carbonates in Eocene to  
710 Quaternary Sediments from the Arctic Ocean and Norwegian-Greenland Sea.  
711 Proceedings of the Ocean Drilling Program, Scientific Results 151.
- 712 Clotten, C., Stein, R., Fahl, K., De Schepper, S., 2018. Seasonal sea ice cover during  
713 the warm Pliocene: Evidence from the Iceland Sea (ODP Site 907). Earth and  
714 Planetary Science Letters 481, 61-72.
- 715 De Schepper, S., Schreck, M., Beck, K.M., Matthiessen, J., Fahl, K., Mangerud, G.,  
716 2015. Early Pliocene onset of modern Nordic Seas circulation related to ocean  
717 gateway changes. Nature Communications 6, 8659.
- 718 Ding, Q., Schweiger, A., L’Heureux, M., Steig, E.J., Battisti, D.S., Johnson, N.C.,  
719 Blanchard-Wrigglesworth, E., Po-Chedley, S., Zhang, Q., Harnos, K., Bushuk,  
720 M., Markle, B., Baxter, I., 2018. Fingerprints of internal drivers of Arctic sea ice  
721 loss in observations and model simulations. Nature Geoscience.
- 722 Dowsett, H., Robinson, M., Haywood, A.M., Salzmann, U., Hill, D., Sohl, L.E., Chandler,  
723 M., Williams, M., Foley, K., Stoll, D.K., 2010. The PRISM3D paleoenvironmental  
724 reconstruction. Stratigraphy 7, 123-139.
- 725 Dowsett, H.J., Cronin, T.M., Poore, R.Z., Thompson, R.S., Whatley, R.C., Wood, A.M.,  
726 1992. Micropaleontological Evidence for Increased Meridional Heat Transport in  
727 the North Atlantic Ocean During the Pliocene. Science 258, 1133-1135.
- 728 Dowsett, H.J., Robinson, M.M., Foley, K.M., 2009. Pliocene three-dimensional global  
729 ocean temperature reconstruction. Clim. Past 5, 769-783.
- 730 Dowsett, H.J., Robinson, M.M., Haywood, A.M., Hill, D.J., Dolan, A.M., Stoll, D.K.,  
731 Chan, W.-L., Abe-Ouchi, A., Chandler, M.A., Rosenbloom, N.A., Otto-Bliesner,

732 B.L., Bragg, F.J., Lunt, D.J., Foley, K.M., Riesselman, C.R., 2012. Assessing  
733 confidence in Pliocene sea surface temperatures to evaluate predictive models.  
734 Nature Climate Change 2, 365.

735 Dubois-Dauphin, Q., Colin, C., Bonneau, L., Montagna, P., Wu, Q., Van Rooij, D.,  
736 Reverdin, G., Douville, E., Thil, F., Waldner, A., Frank, N., 2017. Fingerprinting  
737 Northeast Atlantic water masses using neodymium isotopes. *Geochimica et*  
738 *Cosmochimica Acta* 210, 267-288.

739 Foster, G.L., Royer, D.L., Lunt, D.J., 2017. Future climate forcing potentially without  
740 precedent in the last 420 million years. *Nature Communications* 8, 14845.

741 François, L., Catherine, J., 2004. Neodymium isotopic composition and rare earth  
742 element concentrations in the deep and intermediate Nordic Seas: Constraints  
743 on the Iceland Scotland Overflow Water signature. *Geochemistry, Geophysics,*  
744 *Geosystems* 5.

745 Frank, M., 2002. RADIOGENIC ISOTOPES: TRACERS OF PAST OCEAN  
746 CIRCULATION AND EROSIONAL INPUT. *Reviews of Geophysics* 40, 1-1-1-38.

747 Grøsfjeld, K., De Schepper, S., Fabian, K., Husum, K., Baranwal, S., Andreassen, K.,  
748 Knies, J., 2014. Dating and palaeoenvironmental reconstruction of the  
749 sediments around the Miocene/Pliocene boundary in Yermak Plateau ODP Hole  
750 911A using marine palynology. *Palaeogeography, Palaeoclimatology,*  
751 *Palaeoecology* 414, 382-402.

752 Haley, B.A., Frank, M., Spielhagen, R.F., Eisenhauer, A., 2007. Influence of brine  
753 formation on Arctic Ocean circulation over the past 15 million years. *Nature*  
754 *Geoscience* 1, 68.



755 Haywood, A.M., Dowsett, H.J., Dolan, A.M., 2016. Integrating geological archives and  
756 climate models for the mid-Pliocene warm period. *Nature Communications* 7,  
757 10646.

758 Haywood, A.M., Hill, D.J., Dolan, A.M., Otto-Bliesner, B.L., Bragg, F., Chan, W.L.,  
759 Chandler, M.A., Contoux, C., Dowsett, H.J., Jost, A., Kamae, Y., Lohmann, G.,  
760 Lunt, D.J., Abe-Ouchi, A., Pickering, S.J., Ramstein, G., Rosenbloom, N.A.,  
761 Salzmann, U., Sohl, L., Stepanek, C., Ueda, H., Yan, Q., Zhang, Z., 2013.  
762 Large-scale features of Pliocene climate: results from the Pliocene Model  
763 Intercomparison Project. *Clim. Past* 9, 191-209.

764 Haywood, A.M., Valdes, P.J., 2004. Modelling Pliocene warmth: contribution of  
765 atmosphere, oceans and cryosphere. *Earth and Planetary Science Letters* 218,  
766 363-377.

767 Horikawa, K., Martin, E.E., Basak, C., Onodera, J., Seki, O., Sakamoto, T., Ikehara, M.,  
768 Sakai, S., Kawamura, K., 2015. Pliocene cooling enhanced by flow of low-  
769 salinity Bering Sea water to the Arctic Ocean. *Nature Communications* 6, 7587.

770 Huber, R., Meggers, H., Baumann, K.H., Henrich, R., 2000. Recent and Pleistocene  
771 carbonate dissolution in sediments of the Norwegian–Greenland Sea. *Marine*  
772 *Geology* 165, 123-136.

773 IPCC, 2013. *Climate Change 2013: The Physical Science Basis*. Contribution of  
774 Working Group I to the Fifth Assessment Report of the Intergovernmental Panel  
775 on Climate Change. Cambridge University Press, Cambridge, United Kingdom  
776 and New York, NY, USA.

777 Kinnard, C., Zdanowicz, C.M., Fisher, D.A., Isaksson, E., de Vernal, A., Thompson,  
778 L.G., 2011. Reconstructed changes in Arctic sea ice over the past 1,450 years.  
779 Nature 479, 509.

780 Knies, J., Cabedo-Sanz, P., Belt, S.T., Baranwal, S., Fietz, S., Rosell-Melé, A., 2014a.  
781 The emergence of modern sea ice cover in the Arctic Ocean. Nature  
782 Communications 5, 5608.

783 Knies, J., Matthiessen, J., Vogt, C., Stein, R., 2002. Evidence of ‘Mid-Pliocene (~3 Ma)  
784 global warmth’ in the eastern Arctic Ocean and implications for the  
785 Svalbard/Barents Sea ice sheet during the late Pliocene and early Pleistocene  
786 (~3 – 1.7 Ma). Boreas 31, 82-93.

787 Knies, J., Mattingdal, R., Fabian, K., Grøsfjeld, K., Baranwal, S., Husum, K., De  
788 Schepper, S., Vogt, C., Andersen, N., Matthiessen, J., Andreassen, K., Jokat,  
789 W., Nam, S.-I., Gaina, C., 2014b. Effect of early Pliocene uplift on late Pliocene  
790 cooling in the Arctic–Atlantic gateway. Earth and Planetary Science Letters 387,  
791 132-144.

792 Köseoğlu, D., Belt, S.T., Husum, K., Knies, J., 2018. An assessment of biomarker-  
793 based multivariate classification methods versus the PIP25 index for paleo Arctic  
794 sea ice reconstruction. Organic Geochemistry 125, 82-94.

795 Lacan, F., Jeandel, C., 2004. Denmark Strait water circulation traced by heterogeneity  
796 in neodymium isotopic compositions. Deep Sea Research Part I: Oceanographic  
797 Research Papers 51, 71-82.

798 Lambelet, M., van de Flierdt, T., Crocket, K., Rehkämper, M., Kreissig, K., Coles, B.,  
799 Rijkenberg, M.J.A., Gerringa, L.J.A., de Baar, H.J.W., Steinfeldt, R., 2016.

800 Neodymium isotopic composition and concentration in the western North Atlantic  
 801 Ocean: Results from the GEOTRACES GA02 section. *Geochimica et*  
 802 *Cosmochimica Acta* 177, 1-29.

803 Lang, D.C., Bailey, I., Wilson, P.A., Chalk, T.B., Foster, G.L., Gutjahr, M., 2016.  
 804 Incursions of southern-sourced water into the deep North Atlantic during late  
 805 Pliocene glacial intensification. *Nature Geoscience* 9, 375.

806 Laskar, J., Robutel, P., Joutel, F., Gastineau, M., Correia, A.C.M., Levrard, B., 2004. A  
 807 long-term numerical solution for the insolation quantities of the Earth. *A&A* 428,  
 808 261-285.

809 Laukert, G., Frank, M., Bauch, D., Hathorne, E.C., Rabe, B., von Appen, W.-J., Wegner,  
 810 C., Zieringer, M., Kassens, H., 2017. Ocean circulation and freshwater pathways  
 811 in the Arctic Mediterranean based on a combined Nd isotope, REE and oxygen  
 812 isotope section across Fram Strait. *Geochimica et Cosmochimica Acta* 202, 285-  
 813 309.

814 Lawrence, K., Herbert, T., M. Brown, C., Raymo, M., M. Haywood, A., 2009. High  
 815 amplitude variations in North Atlantic sea surface temperature during the Early  
 816 Pliocene Warm Period.

817 Lisiecki, L.E., Raymo, M.E., 2005. A Pliocene-Pleistocene stack of 57 globally  
 818 distributed benthic  $\delta^{18}\text{O}$  records. *Paleoceanography* 20.

819 Martin, F., 2002. RADIOGENIC ISOTOPES: TRACERS OF PAST OCEAN  
 820 CIRCULATION AND EROSIONAL INPUT. *Reviews of Geophysics* 40, 1-1-1-38.

821 Mattingsdal, R., Knies, J., Andreassen, K., Fabian, K., Husum, K., Grøsfjeld, K., De  
822 Schepper, S., 2014. A new 6 Myr stratigraphic framework for the Atlantic–Arctic  
823 Gateway. *Quaternary Science Reviews* 92, 170-178.

824 Müller, J., Wagner, A., Fahl, K., Stein, R., Prange, M., Lohmann, G., 2011. Towards  
825 quantitative sea ice reconstructions in the northern North Atlantic: A combined  
826 biomarker and numerical modelling approach. *Earth and Planetary Science*  
827 *Letters* 306, 137-148.

828 Müller, J., Werner, K., Stein, R., Fahl, K., Moros, M., Jansen, E., 2012. Holocene  
829 cooling culminates in sea ice oscillations in Fram Strait. *Quaternary Science*  
830 *Reviews* 47, 1-14.

831 Naafs, B.D.A., Stein, R., Hefter, J., Khélifi, N., De Schepper, S., Haug, G.H., 2010. Late  
832 Pliocene changes in the North Atlantic Current. *Earth and Planetary Science*  
833 *Letters* 298, 434-442.

834 Petrie, R.E., Shaffrey, L.C., Sutton, R.T., 2015. Atmospheric Impact of Arctic Sea Ice  
835 Loss in a Coupled Ocean–Atmosphere Simulation. *Journal of Climate* 28, 9606-  
836 9622.

837 Polyakov, I.V., Pnyushkov, A.V., Alkire, M.B., Ashik, I.M., Baumann, T.M., Carmack,  
838 E.C., Goszczko, I., Guthrie, J., Ivanov, V.V., Kanzow, T., Krishfield, R., Kwok,  
839 R., Sundfjord, A., Morison, J., Rember, R., Yulin, A., 2017. Greater role for  
840 Atlantic inflows on sea-ice loss in the Eurasian Basin of the Arctic Ocean.  
841 *Science* 356, 285-291.

842 Prescott, C.L., Dolan, A.M., Haywood, A.M., Hunter, S.J., Tindall, J.C., 2018. Regional  
843 climate and vegetation response to orbital forcing within the mid-Pliocene Warm  
844 Period: A study using HadCM3. *Global and Planetary Change* 161, 231-243.

845 R Core Team, 2018. R: A language and environment for statistical computing. R  
846 Foundation for Statistical Computing. Vienna, Austria URL [http://www.R-](http://www.R-project.org/)  
847 [project.org/](http://www.R-project.org/).

848 Raymo, M.E., Grant, B., Horowitz, M., Rau, G.H., 1996. Mid-Pliocene warmth: stronger  
849 greenhouse and stronger conveyor. *Marine Micropaleontology* 27, 313-326.

850 Rempfer, J., Stocker, T.F., Joos, F., Dutay, J.-C., Siddall, M., 2011. Modelling Nd-  
851 isotopes with a coarse resolution ocean circulation model: Sensitivities to model  
852 parameters and source/sink distributions. *Geochimica et Cosmochimica Acta* 75,  
853 5927-5950.

854 Sato, T., Kameo, K., 1996. Pliocene to Quaternary calcareous nannofossil biostratig-  
855 raphy of the Arctic Ocean, with reference to late Pliocene glaciation. W.F. (Eds.),  
856 *Proc. ODP, Sci. Results* 151.

857 Sharma, M., Basu, A.R., Nesterenko, G.V., 1992. Temporal Sr-, Nd- and Pb-isotopic  
858 variations in the Siberian flood basalts: Implications for the plume-source  
859 characteristics. *Earth and Planetary Science Letters* 113, 365-381.

860 Smik, L., Cabedo-Sanz, P., Belt, S.T., 2016. Semi-quantitative estimates of paleo Arctic  
861 sea ice concentration based on source-specific highly branched isoprenoid  
862 alkenes: A further development of the PIP25 index. *Organic Geochemistry* 92,  
863 63-69.

- 864 Spielhagen, R.F., Werner, K., Sørensen, S.A., Zamelczyk, K., Kandiano, E., Budeus,  
865 G., Husum, K., Marchitto, T.M., Hald, M., 2011. Enhanced Modern Heat Transfer  
866 to the Arctic by Warm Atlantic Water. *Science* 331, 450-453.
- 867 Stein, R., Fahl, K., Gierz, P., Niessen, F., Lohmann, G., 2017. Arctic Ocean sea ice  
868 cover during the penultimate glacial and the last interglacial. *Nature*  
869 *Communications* 8, 373.
- 870 Tachikawa, K., Jeandel, C., Roy-Barman, M., 1999. A new approach to the Nd  
871 residence time in the ocean: the role of atmospheric inputs. *Earth and Planetary*  
872 *Science Letters* 170, 433-446.
- 873 Tanaka, T., Togashi, S., Kamioka, H., Amakawa, H., Kagami, H., Hamamoto, T.,  
874 Yuhara, M., Orihashi, Y., Yoneda, S., Shimizu, H., Kunimaru, T., Takahashi, K.,  
875 Yanagi, T., Nakano, T., Fujimaki, H., Shinjo, R., Asahara, Y., Tanimizu, M.,  
876 Dragusanu, C., 2000. JNdi-1: A neodymium isotopic reference in consistency  
877 with LaJolla neodymium.
- 878 Teschner, C., Frank, M., Haley, B.A., Knies, J., 2016. Plio-Pleistocene evolution of  
879 water mass exchange and erosional input at the Atlantic-Arctic gateway.  
880 *Paleoceanography* 31, 582-599.
- 881 Tütken, T., Eisenhauer, A., Wiegand, B., Hansen, B.T., 2002. Glacial–interglacial cycles  
882 in Sr and Nd isotopic composition of Arctic marine sediments triggered by the  
883 Svalbard/Barents Sea ice sheet. *Marine Geology* 182, 351-372.
- 884 Vogt, C., Knies, J., Spielhagen, R.F., Stein, R., 2001. Detailed mineralogical evidence  
885 for two nearly identical glacial/deglacial cycles and Atlantic water advection to

886 the Arctic Ocean during the last 90,000 years. *Global and Planetary Change* 31,  
887 23-44.

888 Werner, K., Frank, M., Teschner, C., Müller, J., F. Spielhagen, R., 2014. Neoglacial  
889 change in deep water exchange and increase of sea-ice transport through  
890 eastern Fram Strait: Evidence from radiogenic isotopes.

891 Zamelczyk, K., Rasmussen, T.L., Husum, K., Godtliebse, F., Hald, M., 2014. Surface  
892 water conditions and calcium carbonate preservation in the Fram Strait during  
893 marine isotope stage 2, 28.8–15.4 kyr. *Paleoceanography* 29, 1-12.

894 Zhang, Z.S., Nisancioglu, K.H., Chandler, M.A., Haywood, A.M., Otto-Bliesner, B.L.,  
895 Ramstein, G., Stepanek, C., Abe-Ouchi, A., Chan, W.L., Bragg, F.J., Contoux,  
896 C., Dolan, A.M., Hill, D.J., Jost, A., Kamae, Y., Lohmann, G., Lunt, D.J.,  
897 Rosenbloom, N.A., Sohl, L.E., Ueda, H., 2013. Mid-pliocene Atlantic Meridional  
898 Overturning Circulation not unlike modern. *Clim. Past* 9, 1495-1504.

899

900